Journal of Power Sources 239 (2013) 128–131

Contents lists available at SciVerse ScienceDirect

Journal of Power Sources

journal homepage: www.elsevier.com/locate/jpowsour

Short communication

Enhancing the capacitance of TiO_2 nanotube arrays by a facile cathodic reduction process

He Zhou, Yanrong Zhang*

Environmental Science Research Institute, Huazhong University of Science and Technology, Wuhan 430074, China

HIGHLIGHTS

- TiO_2 nanotube arrays were modified by a facile cathodic reduction process.
- Oxygen vacancies were formed and hydroxyls were introduced on the surface of TiO_2.
- The electrochemical activity and conductivity of modified sample were improved.
- The modified sample showed much enhanced capacitance over the pristine one.

ARTICLE INFO

Article history:
Received 10 November 2012
Received in revised form
5 March 2013
Accepted 21 March 2013
Available online 1 April 2013

Keywords:
Titania nanotubes
Cathodic reduction
Supercapacitor
Non-faradic capacitance

ABSTRACT

TiO_2 nanotube arrays are modified by a facile cathodic reduction process treatment and the results are discussed in terms of their electrochemical activity and conductivity. The instrumental characterizations such as X-ray photoelectron spectroscopy and Raman spectroscopy indicate that the formation of oxygen vacancies in the lattice and introduction of hydroxyl groups on the surface of TiO_2 take place. The capacitance of the modified sample is found to be 13 times larger than the pristine TiO_2 nanotube arrays. This work reveals a feasible and simple method to improve electrochemical activity and conductivity of TiO_2 for supercapacitors application.

1. Introduction

Highly ordered TiO_2 nanotube arrays, have attracted much attention, owing to their high regulation, large surface area, excellent controllability and stability [1–3]. In recent years, the focus was made on using TiO_2 nanotube arrays as an active material for potential charge storage device [4–8]. The findings revealed that unlike carbon materials and other metal oxides [9–11], titania capacitors exhibited the behavior of conventional electric double layer capacitors (EDLC) act by a non-faradic mechanism with a very low specific capacitance. The poor capacitive behavior of TiO_2 was found to be mainly due to its low electrochemical activity and high resistance, originated from its semiconductor characteristic. Since the properties of TiO_2 are very sensitive to oxygen content in the lattice [12,13], controlled introduction of oxygen vacancies (Ti^{3+} sites) into the TiO_2 nanotube arrays has been proved to be an effective method to improve its electrochemical activity and conductive behavior of for supercapacitor application [14,15]. However these approaches are always involved in rigorous heat treatment procedure in hydrogen or argon atmosphere, which is not cost-effective considering the extra requirement of instruments and resources.

In this study, a facile cathodic reduction process to introduce oxygen vacancies into the TiO_2 nanotube arrays is investigated and documented. The cathodic reduction process could be carried out for several minutes employing an electrochemical instrument, following the preparation of TiO_2 nanotube arrays by electrochemical anodization. Consequently, compared to the heat treatment routes, the cathodic reduction process is expected to have enhancement on the capacitance along with its user friendly preparation conditions. When the TiO_2 nanotube arrays were treated with the cathodic reduction process, oxygen vacancies were formed and hydroxyl groups were introduced on the surface of TiO_2, leading to highly improved electrochemical activity and conductivity. The reduced TiO_2 nanotube arrays (denoted as R-TNTs) prepared by the simple cathodic process showed enhanced

* Corresponding author. Tel./fax: +86 27 87792101.
E-mail address: yanrong_zhang@hust.edu.cn (Y. Zhang).

0378-7753/$ – see front matter © 2013 Elsevier B.V. All rights reserved.
http://dx.doi.org/10.1016/j.jpowsour.2013.03.114

capacitance over the pristine TiO_2 nanotube arrays (denoted as TNTs).

2. Experimental

2.1. Preparation of TNTs and R-TNTs

The TNTs were prepared by an electrochemical anodization process as per the procedure mentioned in earlier report [16]. The R-TNTs were obtained by electrochemical reduction of the TNTs for 20 min in a two-electrode system at room temperature, employing the TNTs and Pt mesh as cathode and anode respectively. 0.1 M Na_2SO_4 solution was used as supporting electrolyte, and the distance between electrodes was exactly fixed as 4 cm. The applied potential of the cathodic process was maintained in the ranges of +2 to +8 V, and the optimum potential was found to be +4 V.

2.2. Characterization of TNTs and R-TNTs

To investigate the microstructure and composition of the samples, field emission scanning electron microscopy (FE-SEM, NANOSEM 450, FEI), X-ray photoelectron spectroscopy (XPS, XSAM800, KRATOS) with Mg K_α X-ray ($h\nu = 1253.6$ eV) at 12 kV and Raman spectroscopy (HORIBA Jobin Yvon LabRAM) with Ar^+ laser of 514.4 nm excitation were employed.

The electrochemical properties of the samples were investigated with electrochemical impedance spectroscopy (EIS), cyclic voltammetry (CV) and galvanostatic charge–discharge tests by an electrochemical workstation (CS350, CorrTest, China). Experiments were carried out in an undivided compartment with three-electrode system using the TNTs or R-TNTs, saturated calomel electrode (SCE) and Pt mesh as the working, reference, and counter electrodes, respectively. EIS measurements were performed between 100 kHz and 0.01 Hz under a constant potential of −0.1 V (vs. SCE) with a 5 mV rms sinusoidal modulation. The stability of the R-TNTs was investigated by galvanostatic charge–discharge measurement up to 1000 cycles at a current density of 100 μA cm^{-2}. All the electrochemical measurements were performed in a 0.5 M Na_2SO_4 solution at room temperature.

3. Results and discussion

The top and side views of the SEM images were taken for TNTs and R-TNTs. As shown in Fig. 1a, the structure of the R-TNTs consists of highly ordered tubes with inner diameter of 40–70 nm, wall thickness of 10–15 nm and tube length of 700–800 nm, which are in identical dimension with that of TNTs (not shown). Fig. 1b shows the normalized Ti 2p XPS spectra of the samples, in which two broad peaks centered at about 458.5 and 464.3 eV that correspond to the characteristic of Ti $2p_{1/2}$ and Ti $2p_{3/2}$ peaks of Ti^{4+} are observed for both the samples [12,15]. In comparison to the TNTs, the peaks of the R-TNTs show a negative shift in binding energy. By subtracting the Ti 2p spectra of the R-TNTs with TNTs, there are two extra peaks centered at ca. 458.0 and 459.5 eV (Fig. 1b). These two peaks are consistent with the characteristic Ti $2p_{1/2}$ and Ti $2p_{3/2}$ peaks of Ti^{3+} [15,17], confirming the presence of Ti^{3+} state in the R-TNTs. Fig. 1c compares the O 1s XPS spectra of the samples. Both the samples exhibit peak at 529.9 eV that is a characteristic peak of Ti–O–Ti [12]. Additionally, a shoulder peak centered at 531.5 eV with higher intensity for R-TNTs could clearly be observed, which is attributed to Ti–OH species [12,17]. These XPS characterization findings strongly suggest that formation of oxygen vacancies and

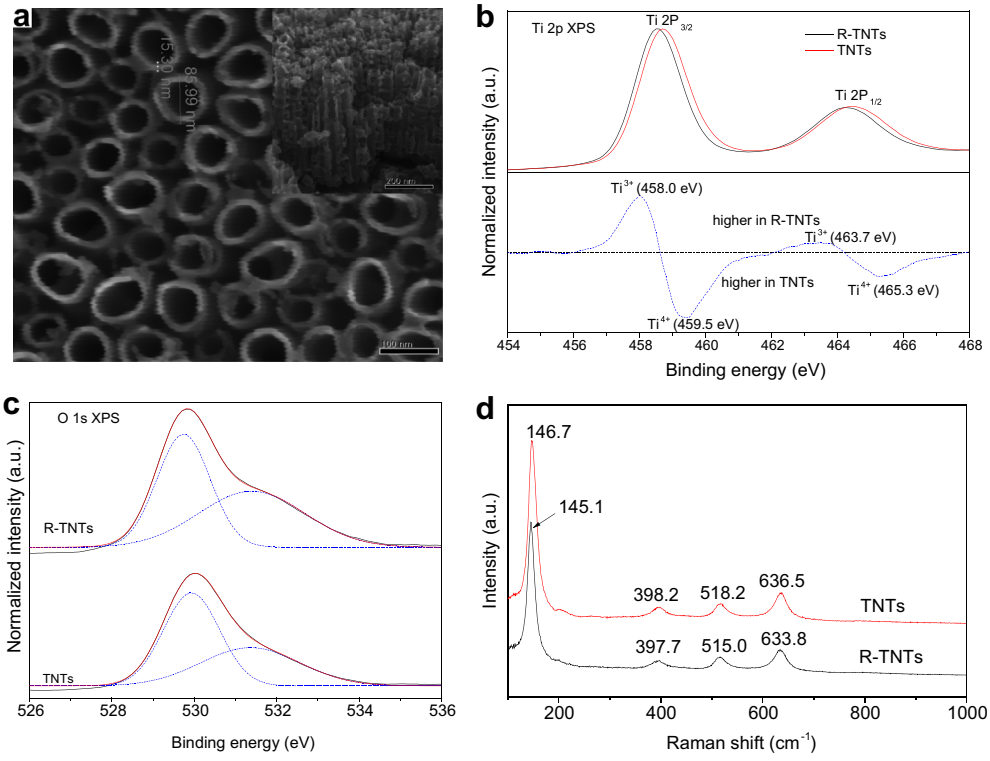

Fig. 1. (a) Typical top view and side view (inset) FE-SEM images of the R-TNTs. (b) Ti 2p XPS spectra of the R-TNTs (black solid line) and TNTs (red solid line), together with their difference spectrum ('R-TNTs' minus 'TNTs', blue dashed line). (c) O 1s XPS spectra of the samples. Black circles are the experimental data, which can be decomposed into a superposition of two peaks shown as blue dashed curves. The red curve is the summation of the two decomposed peaks. (d) Raman spectra of the TNTs and R-TNTs. (For interpretation of the references to colour in this figure legend, the reader is referred to the web version of this article.)

introduction of hydroxyl group on the surface of TNTs take place during the cathodic reduction process. The formation of oxygen vacancies is further confirmed by the Raman spectra (Fig. 1d). The Raman bands of the pristine TNTs, located at 146.7, 398.2, 518.2 and 636.5 cm^{-1}, are attributed to anatase [18]. The Raman peaks of the R-TNTs sample, located at 145.1, 397.7, 515.0 and 633.8 cm^{-1}, show a negative shift compared to the TNTs sample, suggesting the increased amount of oxygen vacancies [14,15].

Typical EIS Nyquist plots with frequencies ranging from 0.01 to 100 kHz are illustrated in Fig. 2a with an inset showing a magnified view of the high frequency regions. For both the samples, Nyquist plots exhibit semicircular arc characteristic, while the plots at the high frequency region start with 45° impedance lines and approach almost vertical lines. These phenomena are completely consistent with the transmission line model [19–21], for which the equivalent circuit representation of the TiO_2 nanotube electrode system is made of a capacitance C, a parallel charge transfer resistance R_{ct} at the solid/electrolyte interface and a series total transport resistance R_{tr}. Compared to the TNTs, the R-TNTs show a bigger diameter semicircle at lower frequency region, indicating a higher value of R_{ct} [22] which signifies a leakage current at the electrode/electrolyte interface and is expected to be as large as possible for a capacitor [23,24]. As a result, the R-TNTs exhibit better parallel combination of R_{ct} and C, showing an approximate vertical line at lower frequency, demonstrate better capacitive characteristic.

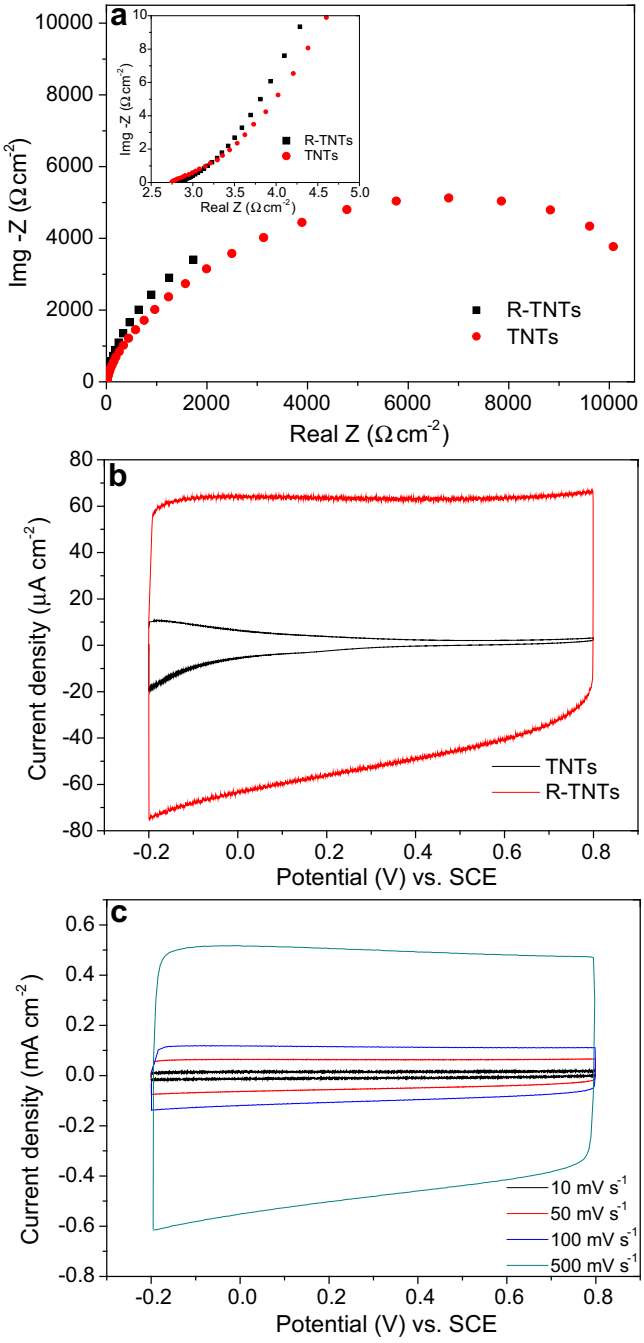

Fig. 2. (a) Nyquist plots of the samples with the inset showing an enlargement of the high frequency regions. (b) CV curves of the samples obtained at a scan rate of 50 mV s^{-1}. (c) CV curves of the R-TNTs scanned at different rates.

Fig. 2b shows the CV curves of the samples recorded at a scan rate of 50 mV s^{-1}. Compared to pristine TNTs, the R-TNTs sample delivers an obvious capacitive characteristic curve close to an ideal rectangular shape [9,23]. Furthermore, the CV curves for R-TNTs exhibit unchanged rectangular shapes as the scan rate increases from 10 to 500 mV s^{-1} (Fig. 2c), indicating good capacitive behavior and high-rate capability of the R-TNTs. Since there is no evidence for any faradic reactions on the rectangular CV curves, it has been deduced that the R-TNTs act as a pure double layer capacitor [9,25]. The cyclic voltammogram shape of EDLC electrodes is affected by the RC time constant (τ) of the electrode system [26]. The ideal rectangular-shaped profile with current decays within an infinitesimally short period after scanning voltage switching indicates quite small RC time constant of the R-TNTs, which is attributed to the increased conductivity of the R-TNTs since the C (in RC) has been highly enlarged.

Fig. 3 is a set of graphs from charge–discharge measurements under galvanostatic conditions. Fig. 3a compares the charge–discharge curves of the TNTs and R-TNTs collected at a current density of 50 μA cm^{-2}. The curve of the R-TNTs electrode is observed to be symmetric and substantially extended over the pristine TNTs electrode, confirming an excellent and enhanced capacitive behavior of the same. Additionally, it shows a small IR drop (0.023 V), again confirming its superior electrical conductive behavior. The relationship between potential and charging–discharging time always keeps good linearity when current density varies from 10 to 100 μA $^{-2}$ for the R-TNTs (Fig. 3b), which is naturally expected from non-faradic electric double layer capacitors [27]. Therefore, it has been deduced that the controlled introduction of oxygen vacancies into the TiO_2 nanotube arrays and hydroxyl groups on TiO_2 surface can improve the electrochemical activity and conductivity of TiO_2 [14,15], leading to enhanced capacitance of the R-TNTs over the pristine TNTs.

Fig. 3c shows the areal capacitance of the samples as a function of current density derived from the charge–discharge test. The areal capacitance of the R-TNTs measured at the current density of 50 μA cm^{-2} is 13 times larger than that of the TNTs, showing much enhanced capacitance. With an increase of charge–discharge current density, the areal capacitance of the R-TNTs gradually decreases as the ion accessibility is limited in the inner region of the porous structure on the relevant timescale [21,28]. The areal capacitance of the R-TNTs measured at a current density of 100 μA cm^{-2} is presented as a function of cycle number in Fig. 3d with the first 10 and the last 10 cycles as insets. From the experimental data, no obvious change could be observed up to 1000 cycles. The decay of areal capacitance was calculated to be 0.7% using the average value of the first 10 and last 10 discharge cycles, which is negligible considering the experimental error. As a result, the R-TNTs electrode exhibits excellent long-term capacitive stability which could be attributed to the pure electric double layer capacitive characteristic.

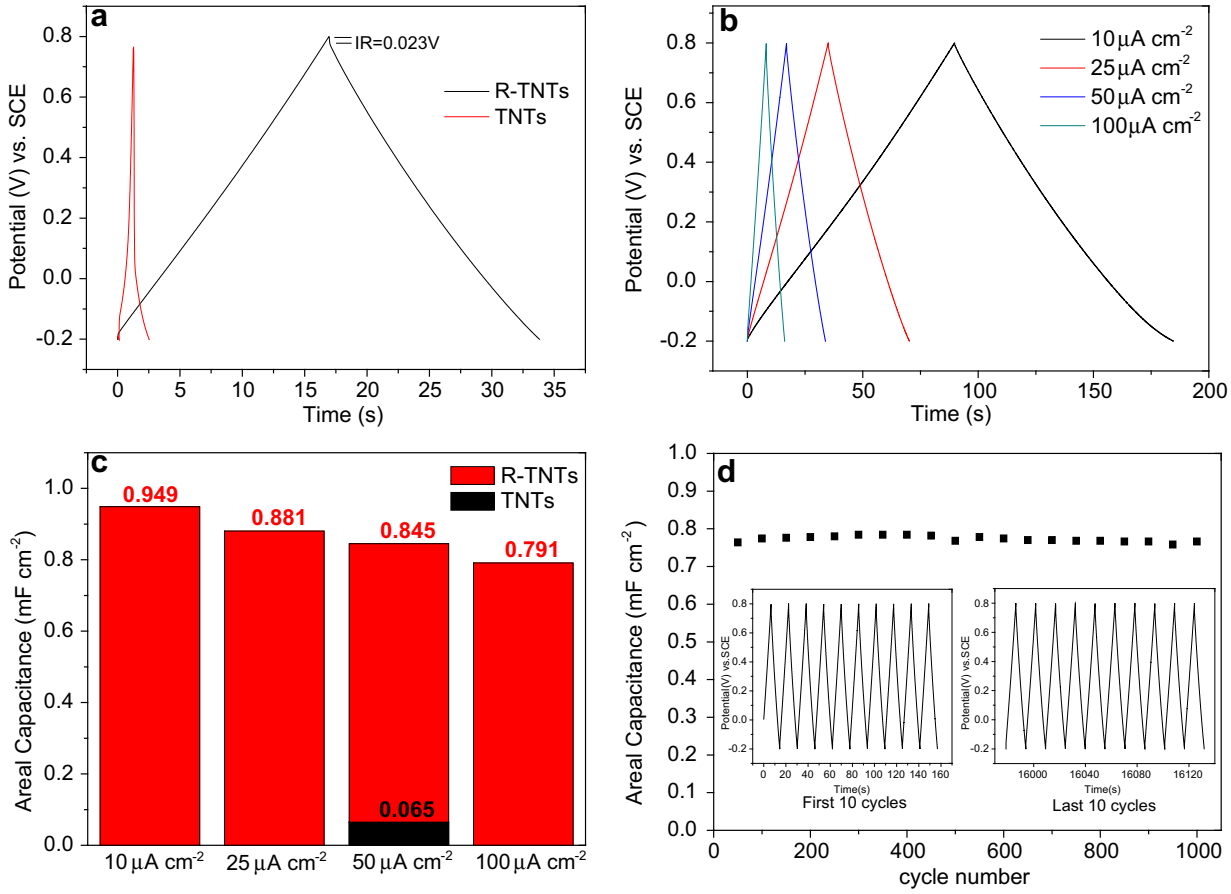

Fig. 3. (a) Galvanostatic charge–discharge plots of the samples collected at a current density of 50 μA cm^{-2}. (b) Galvanostatic charge–discharge plots of the R-TNTs measured as a function of current density. (c) Areal capacitances of the samples derived from the charge–discharge curves measured at different current densities. (d) Areal capacitance of the R-TNTs calculated from charge–discharge test versus cycle number along with first 10 and the last 10 cycles as insets at a current density of 100 μA cm^{-2}.

4. Conclusion

A facile cathodic reduction method was proposed to introduce oxygen vacancies into the TiO_2 nanotube arrays. Improved electrochemical activity, higher conductivity and enhanced capacitance were demonstrated for the modified TNTs (R-TNTs). This method significantly reduces the requirements of instruments and resources compared to the conventional thermal treatment methods, and has a potential application in large-scale productions.

Acknowledgment

This work was supported by Ministry of Science and Technology of China (No. 2010DFA22770), the National Natural Science Foundation of China (No. 51079056/E090301) and the National Science Foundation of Huazhong University of Science and Technology (HUST). The authors thank the Analytical and Testing Center of HUST for the use of SEM, XPS and Raman spectroscopy equipments.

References

[1] K. Shankar, J.I. Basham, N.K. Allam, O.K. Varghese, G.K. Mor, X.J. Feng, M. Paulose, J.A. Seabold, K.S. Choi, C.A. Grimes, Journal of Physical Chemistry C 113 (2009) 6327–6359.
[2] Y. Jun, J.H. Park, M.G. Kang, Chemical Communications 48 (2012) 6456–6471.
[3] J.M. Macak, H. Tsuchiya, A. Ghicov, K. Yasuda, R. Hahn, S. Bauer, P. Schmuki, Current Opinion in Solid State & Materials Science 11 (2007) 3–18.
[4] M.S. Kim, T.W. Lee, J.H. Parka, Journal of the Electrochemical Society 156 (2009) A584–A588.
[5] Y. Xie, L. Zhou, C. Huang, H. Huang, J. Lu, Electrochimica Acta 53 (2008) 3643–3649.
[6] J.H. Kim, K. Zhu, Y.F. Yan, C.L. Perkins, A.J. Frank, Nano Letters 10 (2010) 4099–4104.
[7] M. Salari, S.H. Aboutalebi, K. Konstantinov, H.K. Liu, Physical Chemistry Chemical Physics 13 (2011) 5038–5041.
[8] Y.B. Xie, D.G. Fu, Materials Research Bulletin 45 (2010) 628–635.
[9] P. Simon, Y. Gogotsi, Nature Materials 7 (2008) 845–854.
[10] M.V. Kiamahalleh, S.H.S. Zein, G. Najafpour, S. Abd Sata, S. Buniran, Nano 7 (2012).
[11] A.G. Pandolfo, A.F. Hollenkamp, Journal of Power Sources 157 (2006) 11–27.
[12] X.B. Chen, L. Liu, P.Y. Yu, S.S. Mao, Science 331 (2011) 746–750.
[13] A. Naldoni, M. Allieta, S. Santangelo, M. Marelli, F. Fabbri, S. Cappelli, C.L. Bianchi, R. Psaro, V. Dal Santo, Journal of the American Chemical Society 134 (2012) 7600–7603.
[14] M. Salari, K. Konstantinov, H.K. Liu, Journal of Materials Chemistry 21 (2011) 5128–5133.
[15] X.H. Lu, G.M. Wang, T. Zhai, M.H. Yu, J.Y. Gan, Y.X. Tong, Y. Li, Nano Letters 12 (2012) 1690–1696.
[16] J.Y. Gong, W.H. Pu, C.Z. Yang, J.D. Zhang, Electrochimica Acta 68 (2012) 178–183.
[17] E. McCafferty, J.P. Wightman, Surface and Interface Analysis 26 (1998) 549–564.
[18] X.Y. Pan, X.M. Ma, Journal of Solid State Chemistry 177 (2004) 4098–4103.
[19] F. Fabregat-Santiago, E.M. Barea, J. Bisquert, G.K. Mor, K. Shankar, C.A. Grimes, Journal of the American Chemical Society 130 (2008) 11312–11316.
[20] J. Bisquert, Journal of Physical Chemistry B 106 (2002) 325–333.
[21] D.Y. Qu, H. Shi, Journal of Power Sources 74 (1998) 99–107.
[22] Y.R. Smith, B. Sarma, S.K. Mohanty, M. Misra, Electrochemistry Communications 19 (2012) 131–134.
[23] E. Frackowiak, F. Beguin, Carbon 39 (2001) 937–950.
[24] T. Brezesinski, J. Wang, S.H. Tolbert, B. Dunn, Journal of Sol–Gel Science and Technology 57 (2011) 330–335.
[25] Q.Y. Li, Z.S. Li, L. Lin, X.Y. Wang, Y.F. Wang, C.H. Zhang, H.Q. Wang, Chemical Engineering Journal 156 (2010) 500–504.
[26] S. Yoon, J.W. Lee, T. Hyeon, S.M. Oh, Journal of the Electrochemical Society 147 (2000) 2507–2512.
[27] J. Yan, Z.J. Fan, T. Wei, W.Z. Qian, M.L. Zhang, F. Wei, Carbon 48 (2010) 3825–3833.
[28] D.N. Futaba, K. Hata, T. Yamada, T. Hiraoka, Y. Hayamizu, Y. Kakudate, O. Tanaike, H. Hatori, M. Yumura, S. Iijima, Nature Materials 5 (2006) 987–994.